

Manuscript version: Author's Accepted Manuscript

The version presented in WRAP is the author's accepted manuscript and may differ from the published version or Version of Record.

Persistent WRAP URL:

<http://wrap.warwick.ac.uk/136108>

How to cite:

Please refer to published version for the most recent bibliographic citation information. If a published version is known of, the repository item page linked to above, will contain details on accessing it.

Copyright and reuse:

The Warwick Research Archive Portal (WRAP) makes this work by researchers of the University of Warwick available open access under the following conditions.

© 2020 Elsevier. Licensed under the Creative Commons Attribution-NonCommercial-NoDerivatives 4.0 International <http://creativecommons.org/licenses/by-nc-nd/4.0/>.



Publisher's statement:

Please refer to the repository item page, publisher's statement section, for further information.

For more information, please contact the WRAP Team at: wrap@warwick.ac.uk.

Ga_{2.52}V_{2.48}O_{7.33}(OH)_{0.67}, a Synthetic Member of The Nolanite/Akdalaite-Type Family of Oxyhydroxides Containing Trivalent Vanadium

Daniel S. Cook,¹ Martin R. Lees,² Janet M. Fisher,³ David Thompsett,³ and Richard I. Walton^{1*}

1. Department of Chemistry, University of Warwick, Coventry, CV4 7AL, UK

*Author for correspondence: r.i.walton@warwick.ac.uk

2. Department of Physics, University of Warwick, Coventry, CV4 7AL, UK

3. Johnson Matthey Technology Centre, Sonning Common, Reading, RG4 9NH, UK

Abstract

The oxyhydroxide Ga_{2.52}V_{2.48}O_{7.33}(OH)_{0.67} is prepared by reaction between Ga metal and Na₃VO₄ in a 1:1 monoethanolamine:water mixture at 240 °C. Powder neutron diffraction shows the material to be isostructural with the minerals nolanite and akdalaite, with cations occupying tetrahedral and octahedral interstitial sites in a hexagonal close-packed array of oxide/hydroxide (*P6₃mc*, *a* = 5.7906(2) Å, *c* = 9.2550(5) Å). Rietveld refinement against the data shows that Ga preferentially occupies tetrahedral sites, as well as some octahedral sites, and hence all V is octahedrally coordinated. The oxidation state of vanadium is confirmed as close to V³⁺ using V K-edge X-ray absorption near-edge structure spectroscopy, consistent with the refined chemical composition. The material is metastable, dehydrating around 300 °C and then decomposing above 500 °C, as shown by thermogravimetric analysis and thermodiffraction. The oxide Ga_{2.52}V_{2.48}O₈ produced after dehydration at 300 °C is shown to contain a larger proportion of V⁴⁺ than the parent oxyhydroxide, to ensure charge balance, but the essential hexagonal structure is maintained. Variable temperature magnetisation measurements show that although both materials appear to obey the Curie-Weiss Law at high temperatures, at low temperatures the inverse susceptibility curves are non-linear. There is, however, no evidence for strong magnetic exchange and the extracted effective moments are consistent with the presence of more V³⁺ in the oxyhydroxide compared to the oxide.

Keywords: Solvothermal, gallium, vanadium, oxide, synthesis

1. Introduction

Oxides and oxyhydroxides based on hexagonal close-packed arrays of anions with cations distributed over both tetrahedral and octahedral sites are found in various families of materials. A mixed iron-vanadium oxide belonging to this class of materials is found as the mineral nolanite and was first described in the 1950s by Barnes and Qurashi [1] and by Robinson *et al.* [2], with a chemical formula in the range $\text{Fe}_{2.5}^{2+}\text{V}_{1.7}^{3+}\text{V}_{5.5}^{4+}\text{O}_{16}$ to $\text{Fe}_{2.8}^{2+}\text{V}_{1.5}^{3+}\text{V}_{5.5}^{4+}\text{O}_{16}$ proposed based on chemical analyses of a natural specimen. A crystal structure later reported by Hanson formulated the material as $\text{Fe}_{2.5}^{2+}\text{V}_{1.5}^{3+}\text{V}_6^{4+}\text{O}_{16}$ who provided an analogy with known ternary oxides of tetravalent molybdenum, $\text{A}_2^{2+}\text{Mo}_3^{4+}\text{O}_8$, but without the metal-metal bonding seen in the latter [3]. A subsequent study of a sample of a mineral specimen of nolanite, from Kalgoorlie in Western Australia, was reported in 1983 [4]. This sample contained iron and vanadium but also small amounts of titanium and aluminium, and the composition $(\text{Al,Fe,Ti,V})_{10}\text{O}_{14}(\text{OH})_2$, was deduced, *i.e.* an oxyhydroxide, rather than an oxide, with Al^{3+} , Ti^{4+} and V^{3+} found preferentially to occupy octahedral sites, and a mixture of Fe^{2+} and Fe^{3+} over both tetrahedral and octahedral sites. Other minerals with related structures include $\text{Fe}_2\text{Mo}_3\text{O}_8$ (kamiokite) [5] and $(\text{Mg}_{1.57}\text{Fe}_{0.43})\text{Mo}_3\text{O}_8$ (majindeite) [6]. These studies of natural specimens demonstrate the flexibility of the structure to accommodate various types and distributions of cations, and the possibility of inclusion of hydroxide in place of some of the oxide. In the laboratory, a synthetic example of nolanite has been prepared to investigate magnetic and electronic properties: $\text{Fe}_{2.5}\text{V}_{1.5}\text{V}_{5.6}\text{O}_{16}$ was produced in a nanocrystalline form *via* solvothermal synthesis and was shown to be a magnetic semiconductor with a metal-insulator phase transition below 150 K [7].

The aluminium oxyhydroxide $\text{Al}_5\text{O}_7(\text{OH})$ (often reported as $5\text{Al}_2\text{O}_3 \cdot \text{H}_2\text{O}$ in the literature) is found as the mineral akdalaite [8], was originally synthesised in the laboratory where it was named tohdite [9, 10], and has a related structure to nolanite [11]. Akdalaite has also been discussed as a model for the nanocrystalline iron oxyhydroxide ferrihydrite whose structure was unresolved for a long period of time [12, 13]. Some of us recently reported the gallium analogue of this material, crystallised in a solvothermal reaction between gallium metal and water-diethanolamine mixed solvent [14]. In further work, we showed how mixed-metal gallium oxide spinels could be formed under similar conditions by inclusion of transition-metal salts in the solution, containing either Co [15] or Fe [16]. In the present work, we have extended

this synthetic methodology to include vanadium salts in the solvothermal oxidation of gallium, and in doing so now report a synthetic mixed vanadium-gallium analogue of nolanite.

2. Experimental

2.1 Materials Synthesis

0.150 g (2.15 mmol) of Ga metal (Alfa-Aesar, 99.9%) and 0.396 g (2.15 mmol) Na_3VO_4 (Alfa-Aesar, 99.9%) were added to a 10 ml mixture of 1:1 (vol:vol) water:monoethanolamine (MEA) with stirring. The mixture was sealed in a 23 ml PTFE-lined steel autoclave and heated at 240 °C for 96 hours in a preheated fan-assisted oven. The autoclave was cooled to room temperature naturally and the solid isolated by suction filtration. The black solid was then washed with methanol and dried overnight at 70 °C.

Another synthesis route investigated was based on our recent work used to prepared mixed-metal spinel oxides using metal acetylacetonates as precursors [17]: 0.40 g (1.09 mmol) of $\text{Ga}(\text{acac})_3$ (Aldrich, 99.99%) and 0.380 g (1.09 mmol) $\text{V}(\text{acac})_3$ (Aldrich, 97%) in 10 ml 1,4-butanediol with stirring. This mixture was sealed in a 23 ml PTFE lined autoclave and placed in a preheated fan-assisted oven at 240 °C for 96 hours. Upon cooling naturally to room temperature, the slurry was collected via centrifugation followed by washing in acetone and isolated by further centrifugation. The product was dried overnight at 70 °C to yield a black powder. Although the synthesis was successful, the material prepared by this synthesis route was found to be less crystalline than the method in 1:1 MEA:H₂O (Supporting Information) and so was not studied further.

For comparison, a sample of $\text{Ga}_5\text{O}_7(\text{OH})$ was prepared as in our previous work [14].

2.2 Laboratory Characterisation

Powder X-ray diffraction (XRD) patterns were recorded at room temperature using a Panalytical X'Pert Pro MPD operating with monochromatic $\text{Cu K}\alpha_1$ radiation and equipped with a PIXcel solid-state detector. Full pattern analysis of powder patterns was performed using the Pawley method within the TOPAS software to determine lattice parameters [18]. A Bruker D8 Advance powder diffractometer operating with $\text{Cu K}\alpha_{1/2}$ radiation and equipped with a VÅNTEC-1 solid-state detector with an Anton Parr XRK900 chemical reaction chamber was used to collect powder XRD with *in situ* heating. A typical data collection involved heating from 30 °C to 810 °C or 900 °C at 10 °C min⁻¹ with 30 °C intervals holding for 300 seconds at each interval prior to data collection to allow the temperature to equilibrate.

Scanning electron microscopy (SEM) images were recorded using a ZEISS GEMINI instrument. A small amount of sample was placed on to a carbon tape prior to analysis. Energy-dispersive X-ray analysis (EDXA) was performed on the SEM using a large area SDD EDX detector.

Inductively-coupled plasma optical emission spectroscopy (ICP-OES) analysis for metals was performed after acid digestion by MEDAC Ltd (UK).

Thermogravimetric analysis (TGA) coupled with differential scanning calorimetry (DSC) and mass spectrometry (MS) was used to determine mass loss in samples upon heating in air from room temperature to 1000 °C. A Mettler Toledo TGA/DSC 1-600 instrument equipped with a Hiden HPR-20 QIC R&D specialist gas analysis system, a triple filter mass spectrometer with SEM detection was used.

Magnetic properties were studied using a Quantum Design Magnetic Property Measurement System (MPMS) magnetometer. Each sample (10 to 20 mg) was placed in a gel capsule and in turn placed in a plastic straw. Magnetisation, M , versus applied field, H , data were collected at 5 and 300 K. Magnetic susceptibility ($\chi = M/H$) measurements were made between 2 and 380 K in an applied field of 1000 Oe.

2.3 Time-of-flight neutron diffraction

Time-of-flight powder neutron diffraction data were collected on the Polaris instrument, at ISIS, the UK's neutron spallation source [19], at room temperature. The sample was dried in a vacuum oven overnight prior to data collection to remove any surface contaminants (in particular surface bound water or organic molecules) to minimise the incoherent scattering from the protons associated with these contaminants. The sample was loaded into a vanadium can of 6 mm diameter, which was placed inside an evacuated chamber. Rietveld refinements of structural models against the neutron diffraction data were performed using TOPAS implemented with jEdit [18]. Data from Bank 3 (~0.33 – 7.0 Å) and from Bank 5 (~0.15 to 2.7 Å) of Polaris were used and the structural model refined simultaneously against each dataset. The incoherent scattering due to the protons present was refined as part of the smooth background in the diffraction profiles.

2.4 X-ray absorption near-edge spectroscopy

X-ray absorption near-edge structure (XANES) spectroscopy was performed on Beamline B18 at the Diamond Light Source, UK [20] in order to probe the oxidation state and local

coordination environment of vanadium in the materials. The samples were diluted with polyethylene powder and then pressed into thin pellets of 13 mm diameter and approx. 1 mm thick. Absorption data were collected at the vanadium K-edge in transmission mode, and spectra were normalised using the program ATHENA [21].

3. Results and discussion

The room temperature powder XRD pattern of the material formed in MEA:H₂O, Figure 1, shows reflections with two clearly different peak shapes. Upon indexing, however, an hexagonal unit cell was found, with lattice parameters $a = 5.78 \text{ \AA}$, $c = 9.28 \text{ \AA}$, analogous to the Al₅O₇(OH)-type structure (akdalaite) [10] and the pure gallium analogue, Ga₅O₇(OH), that has lattice parameters $a = 5.82107(8) \text{ \AA}$, $c = 9.0662(2) \text{ \AA}$ [14]. The two distinct peak shapes found in the powder pattern of the new vanadium material are a clear example of anisotropic peak broadening often found for materials composed of plate morphology. The intense sharp peaks however indicate that the material has a large crystallite size.

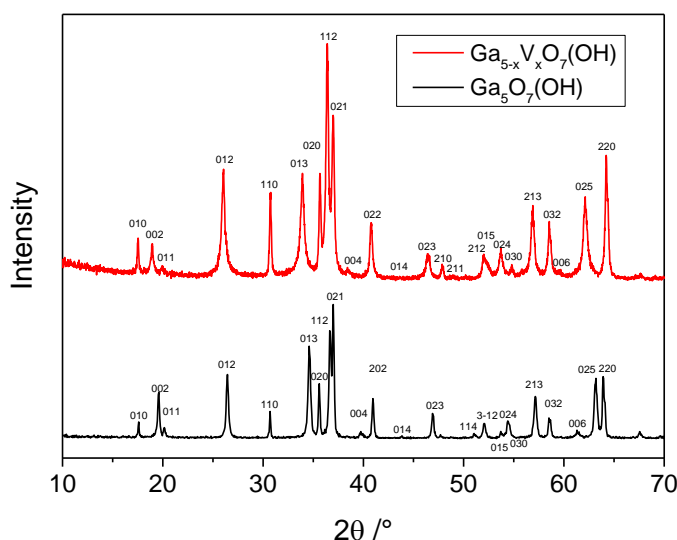


Figure 1 Powder XRD patterns of Ga₅O₇(OH) (lower, black), and the new vanadium substituted gallium oxyhydroxide (upper, red).

Imaging by SEM reveals two distinct particle sizes in the vanadium gallium oxyhydroxide: large clusters of thin plates, and isolated regions of larger plates (Figure 2). Electron microscopy was also used to estimate the ratio of gallium and vanadium in the material: EDXA by SEM suggests that the metal ratio is close to 1:1 (Table 1).

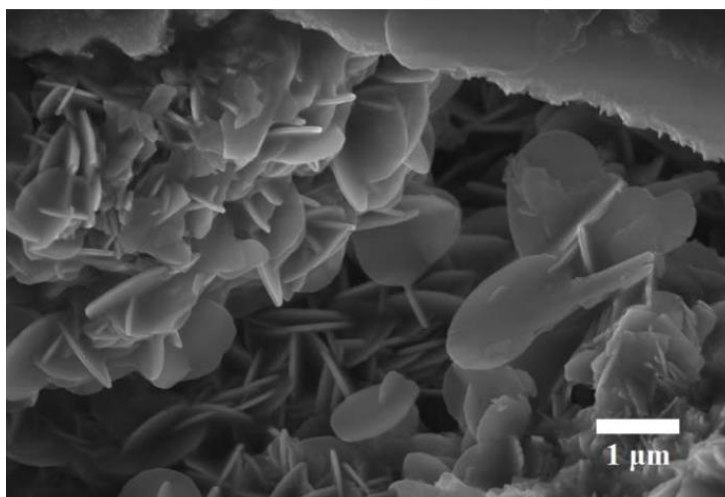


Figure 2 SEM image of $\text{Ga}_{2.52}\text{V}_{2.48}\text{O}_{7.33}(\text{OH})_{0.67}$ showing clusters of plates.

Table 1 Percentage metal content obtained from elemental analysis using electron microscopy, ICP-OES, compared with the value refined from powder neutron diffraction. For the EDXA the estimated errors are high, as expected for this method, for ICP the errors were estimated using a typical experimental error of $\pm 0.3\%$ on quoted mass percentages of metals assayed, and the neutron diffraction values are determined from the statistical errors on refined site occupancies.

Metal	EDX (SEM)	ICP-OES	Refined from neutron powder diffraction
Ga	50.2 ± 5	53.1(2)	50.5(5)
V	49.8 ± 5	46.9(2)	49.5(5)

To determine the crystal structure of the new material, time-of-flight powder neutron diffraction data were recorded: this was to allow refinement of cation site occupancy for the two metals with similar atomic numbers and also to include the protons anticipated in the crystal structure. An initial model using the $\text{Ga}_5\text{O}_7(\text{OH})$ structure was used to fit the data [14]. Vanadium was added to the structure so that the gallium and vanadium initially occupied each site equally to give a Ga:V ratio of 1:1, as expected from the ratio used in the synthesis and inferred from the metal ratios obtained from EDX, (SEM) and bulk analysis using ICP-OES, Table 1.

The structure of akdalaite/tohdite has previously been scrutinised using computational methods to confirm that the space group $P6_3mc$ is adequate: the two subgroups $P31c$ and $Cmc2_1$ offer additional degrees of freedom, but it was found that these are not exploited in akdalaite, with minimal energy differences between all three space groups and that $P6_3mc$ is appropriate [22]. Based on this and the structural refinement of $Ga_5O_7(OH)$, also refined in $P6_3mc$ [14], this space group was chosen for the current work. Two constraints were applied to the refinement. The first was to keep the metal sites fully occupied (*i.e.* so that the total site occupancy equalled 1). The second was to keep the thermal parameter for each mixed metal site the same. Since the coherent scattering cross section of vanadium is 0.018 barns, the structural information of the metal sites will be dominated by gallium. During the refinement, it was found that if the Ga3 (2b) site occupancy was allowed to vary it refined slightly above 1, to 1.019, which was a strong indication that this site was occupied only by gallium and later in the refinement this parameter was fixed at 1.0 to give a meaningful interpretation to the refinement. Stephens' phenomenological model of anisotropic peak broadening was required in order to obtain a satisfactory fit. With the Stephens' parameters used the refinement proceeded to an wR_p of 2.026%, and the refined crystal parameters are shown in Table 2 while the fits to the data from Polaris Banks 3 and 5 are shown in Figure 3.

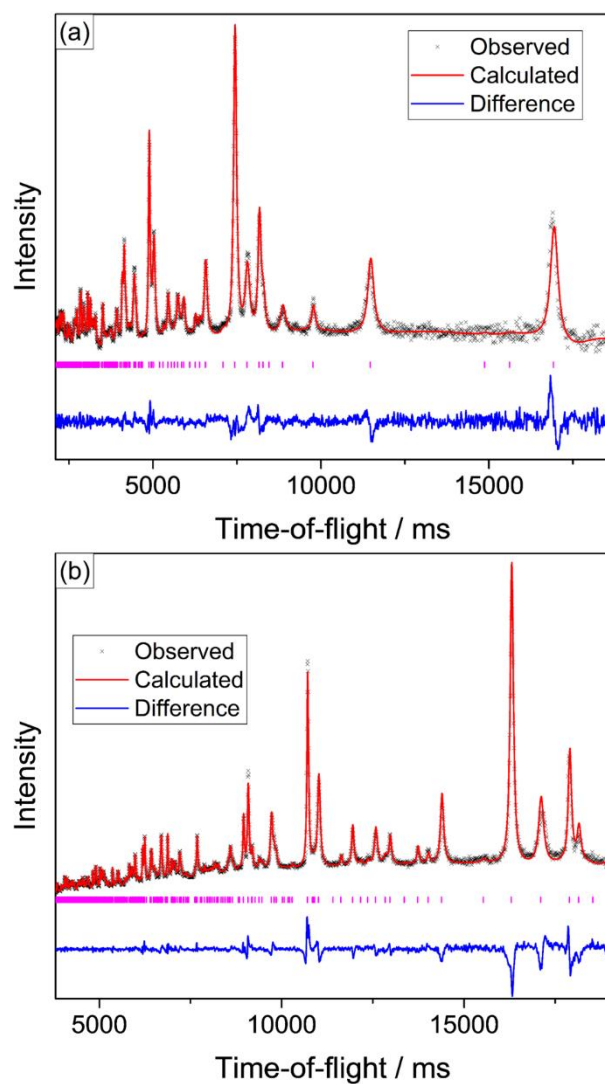


Figure 3 Results of Rietveld refinement of vanadium substituted gallium tohdite using neutrodiffraction from Polaris (a) Bank 3 (d -spacing range: 0.33 – 7 Å) and (b) Bank 5 (d -spacing range 0.1 – 2.65 Å).

Table 2: Refined crystal parameters for $\text{Ga}_{2.52}\text{V}_{2.48}\text{O}_{7.33}(\text{OH})_{0.67}$. Space group $P6_3mc$, $a = 5.7906(2)$ Å, $c = 9.2550(5)$ Å. $R_p = 1.955\%$, $wR_p = 2.026\%$.

Wyckoff site	Atom	x	y	z	Occupancy	Beq / Å ²
6c	Ga1	0.1674(7)	0.3348(14)	0.3440(5)	0.284(7)	0.23(9)
	V1	0.1674(7)	0.3348(14)	0.3440(5)	0.716(7)	0.23(9)
2b	Ga2	2/3	1/3	0.1358(5)	0.671(1)	0.26(7)
	V2	2/3	1/3	0.1358(5)	0.329(1)	0.26(7)
2b	Ga3	1/3	2/3	0.0353(2)	1.0	0.08(2)
2a	O1	0	0	-0.0196(5)	1.0	0.382(12)
6c	O2	0.5127(1)	0.0253(3)	-0.0125(4)	1.0	0.382(12)
6c	O3	0.8310(4)	0.6619(8)	0.2456(4)	1.0	0.382(12)
2b	O4	1/3	2/3	0.2400(5)	1.0	0.382(12)
2a	H1	0	0	0.070(16)	0.67(4)	1.2(2)

The refined chemical composition $\text{Ga}_{2.52}\text{V}_{2.48}\text{O}_{7.33}(\text{OH})_{0.67}$ gives a refined composition close to Ga:V as 1:1 which is in good agreement with both the stoichiometry of the reaction and the metal ratio as inferred from both EDX from electron microscopy and ICP-OES analysis. In addition to this, the tetrahedral site is exclusively occupied by gallium, which is not unexpected owing to the tetrahedral site preference shown by gallium in many oxide materials [23-26]. The octahedral sites are occupied by both gallium and vanadium. The occupancy of the hydrogen refined to 0.67, which is acceptable so long as a small portion of the vanadium is oxidised to V^{4+} . The average oxidation state of vanadium in this model is $\text{V}^{3.13+}$ *i.e.* most of the vanadium is trivalent. V^{3+} is expected preferentially to adopt octahedral coordination owing to its size and crystal field stabilisation energy, such as is found in many spinels [27]. This is in contrast to published nolanite crystal structures that have similar crystal structures to tohdite and where V^{3+} has been found distributed over both the octahedral and tetrahedral sites [2, 4]. For the material studied here, the tetrahedral preference of Ga is presumably the dominant factor dictating the distribution of cations. The oxidation state of vanadium was confirmed using bond valence sums [28]: this gave values of 3.04 and 3.03 for V1 and V2, respectively.

The structure of $\text{Ga}_{2.52}\text{V}_{2.48}\text{O}_{7.33}(\text{OH})_{0.67}$ can be compared to isostructural materials in the nolanite/akdalaite family. The structure consists of hexagonal close packed oxide layers, a layer of $(\text{Ga1}, \text{Va1})\text{O}_6$ octahedra and a layer containing $(\text{Ga2}, \text{V2})\text{O}_6$ octahedra and $(\text{Ga3})\text{O}_4$

tetrahedra, Figure 4. The layers of edge-sharing $(\text{Ga1}, \text{Va1})\text{O}_6$ octahedra also share edges with the $(\text{Ga2}, \text{V2})\text{O}_6$ octahedra in the layer above and below, and corner-share with the $(\text{Ga3})\text{O}_4$ tetrahedra in the layer above and below. Table 3 summarises the relative occupancy of tetrahedral and octahedral sites in some related materials.

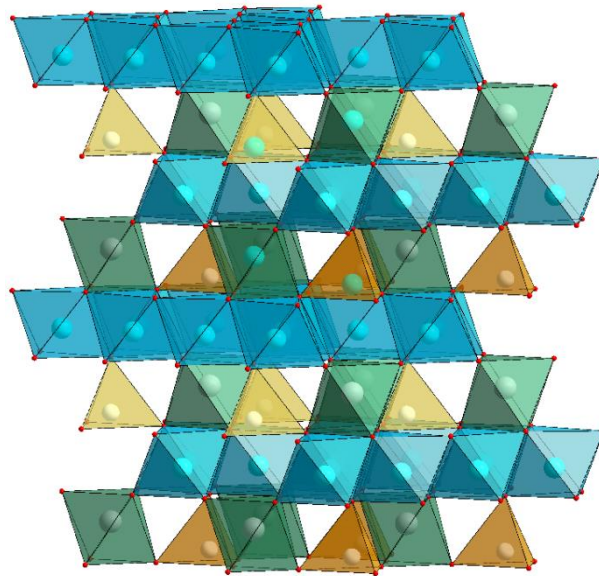


Figure 4: Polyhedral view of the structure of $\text{Ga}_{2.52}\text{V}_{2.48}\text{O}_{7.33}(\text{OH})_{0.67}$. Blue octahedra are the Ga1/V1 sites, green octahedra are Ga2/V2 sites and orange tetrahedra Ga3 sites.

Table 3: Comparison of the composition and site occupancy of $\text{Ga}_{2.52}\text{V}_{2.48}\text{O}_{7.33}(\text{OH})_{0.67}$ with related materials. The superscripts [4] and [6] denote tetrahedral and octahedral sites, respectively.

Material	Chemical formula with site occupation	Reference
$\text{Fe}_{2.5}\text{V}_{1.5}\text{V}_6\text{O}_{16}$ nolanite	$(\text{Fe}^{2+}_{0.78}\text{V}^{3+}_{0.22})_2^{[6]}(\text{Fe}^{2+}_{0.47}\text{V}^{3+}_{0.53})_2^{[4]}(\text{V}^{4+})_6^{[6]}\text{O}_{16}$	[3]
$(\text{Al,Fe,Ti,V})_{10}\text{O}_{14}(\text{OH})_2$ nolanite	$(\text{Al}^{3+}_{0.0375}\text{Fe}^{3+}_{0.025}\text{Ti}^{4+}_{0.075}\text{V}^{3+}_{0.86})_2^{[6]}(\text{Fe}^{2+}_{0.3}\text{Fe}^{3+}_{0.7})_2^{[4]}(\text{Al}^{3+}_{0.0375}\text{Fe}^{3+}_{0.025}\text{Ti}^{4+}_{0.075}\text{V}^{3+}_{0.86})_6^{[6]}\text{O}_{14}(\text{OH})_2$	[4]
$(\text{Al,Fe,Ti,V})_{10}\text{O}_{14}(\text{OH})_2$ nolanite	$(\text{Al}^{3+}_{0.025}\text{Fe}^{3+}_{0.125}\text{Fe}^{2+}_{0.0625}\text{Ti}^{4+}_{0.1375}\text{V}^{3+}_{0.65})_2^{[6]}(\text{Fe}^{2+}_{0.3}\text{Fe}^{3+}_{0.7})_2^{[4]}(\text{Al}^{3+}_{0.025}\text{Fe}^{3+}_{0.125}\text{Fe}^{2+}_{0.0625}\text{Ti}^{4+}_{0.1375}\text{V}^{3+}_{0.65})_6^{[6]}\text{O}_{14}(\text{OH})_2$	[4]
$\text{Al}_5\text{O}_7(\text{OH})$ akdalaite	$(\text{Al}^{3+})_2^{[6]}(\text{Al}^{3+})_2^{[4]}(\text{Al}^{3+})_6^{[6]}\text{O}_{14}(\text{OH})_2$	[11]
$\text{Ga}_5\text{O}_7(\text{OH})$	$(\text{Ga}^{3+})_2^{[6]}(\text{Ga}^{3+})_2^{[4]}(\text{Ga}^{3+})_6^{[6]}\text{O}_{14}(\text{OH})_2$	[14]
$\text{Ga}_{2.52}\text{V}_{2.48}\text{O}_{7.33}(\text{OH})_{0.67}$	$(\text{Ga}^{3+}_{0.67}\text{V}^{3.1+}_{0.33})_2^{[6]}(\text{Ga}^{3+})_2^{[4]}(\text{Ga}^{3+}_{0.28}\text{V}^{3.1+}_{0.72})_6^{[6]}\text{O}_{14.66}(\text{OH})_{1.33}$	this work

The formation of an oxyhydroxide that contains predominantly V^{3+} from a V^{5+} -containing precursor is noteworthy. Control reactions using either only $Ga(acac)_3$ or $V(acac)_3$ under solvothermal reaction conditions yielded β - Ga_2O_3 or corundum-type V_2O_3 , respectively. In the solid-state, a flow of H_2 or CO is typically required to form V_2O_3 by reduction of V_2O_5 [29], VO_2 [30], or other precursors [31]. V_2O_3 has also been prepared solvothermally in amine-water mixtures [32] or by a reflux method from a glycolate precursor [33]. For our material, the long reaction time of 96 hours is necessary in order to obtain a highly crystalline, phase pure material and shorter reaction times gave materials of poor crystallinity. The ~1:1 ratio of metals appears to be fixed: addition of less Na_3VO_4 leads to the presence of $Ga_5O_7(OH)$ as a secondary phase, whilst addition of more Na_3VO_4 yields an unidentified material as one of the products, even after 96 hours.

The presence of hydroxide ions in the solid product was confirmed using infrared spectroscopy (Supporting Information), while thermogravimetric analysis shows the loss of water above 300 °C, consistent with the presence of structural hydroxide (Supporting Information), and reveals a mass loss of 1.2%, which is consistent with conversion of oxyhydroxide to an oxide $Ga_{2.52}V_{2.48}O_8$ (expected mass loss 1.4%). *In situ* powder XRD measured during heating shows that upon heating to 300 °C several peaks shift to higher angle indicating a contraction of the cell which very slowly expands again on further heating (likely due to thermal expansion) up until 600 °C at which point the structure begins to collapse with expulsion of other phase(s) (Figure 5). Kappa and beta gallium oxide are likely candidates for the decomposition phases, and κ - Ga_2O_3 is especially likely since in the contour map a transient phase between 550 – 800 °C is observed, which is analogous to the thermal decomposition of $Ga_5O_7(OH)$ [14]. It is not possible to identify any vanadium decomposition phases with any certainty in the room temperature pattern after firing to 810 °C. The likely explanation for the contraction of the unit cell is removal of the hydroxyl group which would require the vanadium to be oxidised in order to charge balance the structure giving a proposed formula of $Ga_{2.52}V_{2.48}O_8$. The presence of V^{4+} would give shorter V-O bonds than V^{3+} and hence could explain the observed contraction in the unit cell. That the dehydroxylated material is metastable and decomposes around 600 °C suggests that it is unlikely that it could be prepared by conventional high temperature synthesis.

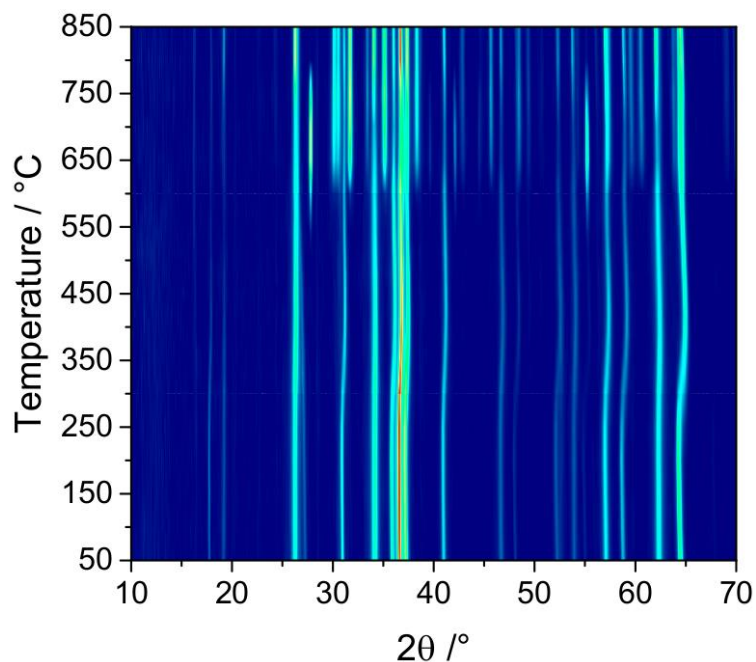


Figure 5 *In situ* X-ray thermodiffractometry measured on heating $\text{Ga}_{2.52}\text{V}_{2.48}\text{O}_{7.33}(\text{OH})_{0.67}$ showing a contraction of the cell occurring around 250 °C – 450 °C. Phase separation occurs around 600 °C and transient phases are observed between 550 °C – 750 °C.

A separate sample was heated to 300 °C for 4 hours and then cooled to room temperature in order to analyse the structure of this material after the period of cell contraction. Infrared spectroscopy confirms that the O-H stretching mode is now absent (Supporting Information). The room temperature powder XRD pattern after firing to 300 °C of this material shows that the material retains its structure after dehydroxylation, Figure 6. A Pawley fit to the pattern, confirms the contraction of the unit cell, Table 4.

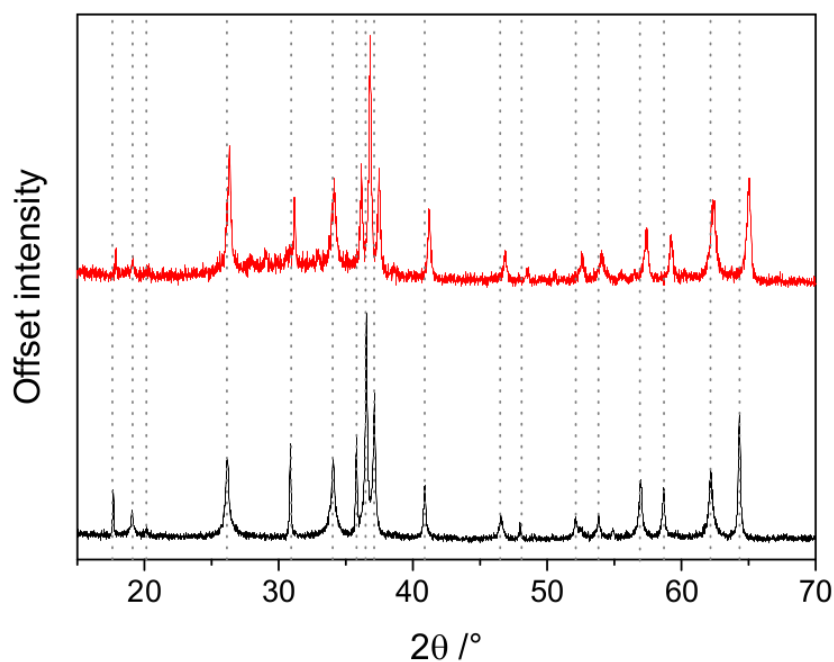


Figure 6 PXRD of as-made $\text{Ga}_{2.52}\text{V}_{2.48}\text{O}_{7.33}(\text{OH})_{0.67}$ (lower, black) and after firing to 300 °C (upper, red). Grey dotted lines highlight the shift of Bragg peaks to high angles after firing, indicating a unit cell contraction.

Table 4 Lattice parameters obtained from Pawley refinement of powder XRD data of $\text{Ga}_{2.52}\text{V}_{2.48}\text{O}_{7.33}(\text{OH})_{0.67}$ before and after heating to 300 °C and during *in situ* thermodiffraction.

	$a / \text{Å}$	$c / \text{Å}$	$V / \text{Å}^3$
As-made sample	5.78824(3)	9.2786(8)	269.22(2)
After firing to 300 °C	5.7492(12)	9.260(3)	265.06(11)
<i>In situ</i> 300 °C	5.7796(16)	9.274(3)	268.28(14)

The oxidation state of vanadium was examined using XANES at the vanadium K-edge along with reference materials, Figure 7. Analysis of the spectra showed that in $\text{Ga}_{2.52}\text{V}_{2.48}\text{O}_{7.33}(\text{OH})_{0.67}$ the calculated oxidation state of vanadium is $\text{V}^{3.11+}$. This agrees excellently with the expected oxidation state of vanadium in the structural model obtained by Rietveld refinement of powder neutron, which requires vanadium to be $\text{V}^{3.13+}$. The presence of a small amount of V^{4+} is hardly surprising: V^{3+} compounds are typically unstable in air (V_2O_3 oxidises slowly in air to VO_2 ; most aqueous V^{3+} cations oxidise to the stable VO^{2+} species [29]). XANES was also measured on a sample that had been heated to 300 °C for 1 hour in air,

which showed a higher oxidation state of $V^{3.40+}$. This is in agreement with observed data from IR, *in situ* thermodiffraction and TGA-MS: these show that at an elevated temperature the oxyhydroxide is dehydrated requiring the vanadium to be partially oxidised in order to charge balance the structure and is entirely consistent with the expected formula $Ga_{2.52}V_{2.48}O_8$, which gives an average oxidation state of vanadium as $V^{3.40+}$. On continued heating structure collapse occurs above 600 °C,

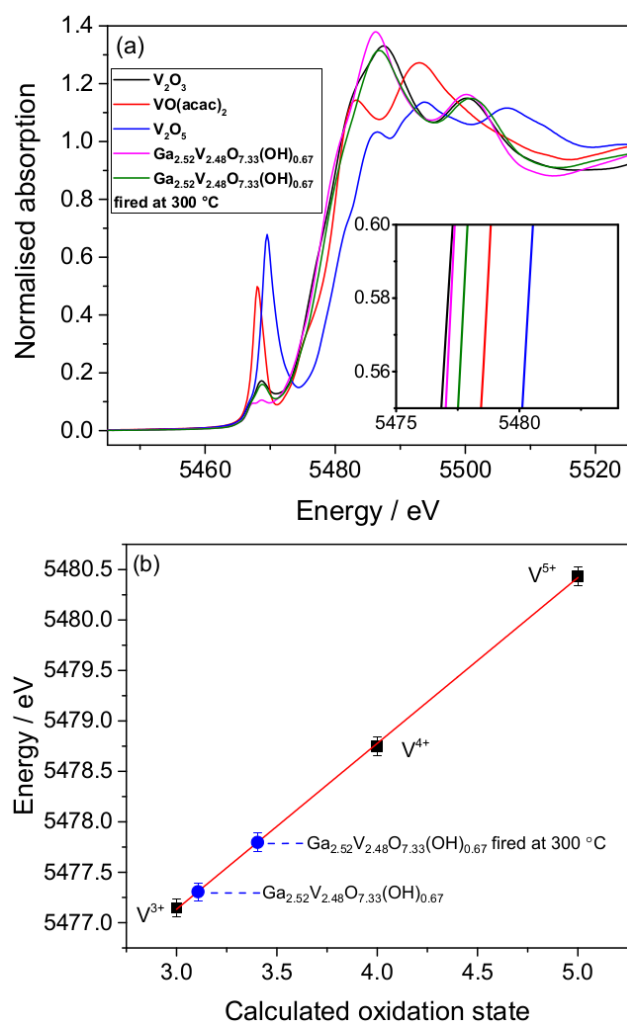


Figure 7 (a) V K-edge XANES spectra normalised to the edge step of $Ga_{2.52}V_{2.48}O_{7.33}(OH)_{0.67}$ before and after firing and relevant references (inset shows a close up of the edge position for all materials), (b) plot of edge position (defined as the energy at which normalised absorption = 0.5) as a function of oxidation state with a linear fit to reference materials providing the calculated oxidation of vanadium in $Ga_{2.52}V_{2.48}O_{7.33}(OH)_{0.67}$ and $Ga_{2.52}V_{2.48}O_{7.33}(OH)_{0.67}$ fired at 300 °C (both in blue).

The temperature dependence of the molar magnetic susceptibility of both the oxyhydroxide $Ga_{2.52}V_{2.48}O_{7.33}(OH)_{0.67}$ and the oxide $Ga_{2.52}V_{2.48}O_8$ are shown in Figure 8. The data include a

temperature independent diamagnetic contribution, χ_0 , and an almost temperature independent contribution, that appears to be paramagnetic, from the sample holder (gel capsule and plastic straw). The diamagnetic contribution was estimated by summing Pascal's constants for the constituent ions [34] and is approximately $(-1.4 \pm 0.1) \times 10^{-4} \text{ emu mol}^{-1}$ for both materials. The background contribution from the sample holder was subtracted from the raw response curves produced by the MPMS magnetometer prior to any normalisation for the formula weight of the samples [35]. This contribution, when normalised for the formula weight, is of the order $(+1.2 \pm 0.1) \times 10^{-4} \text{ emu mol}^{-1}$.

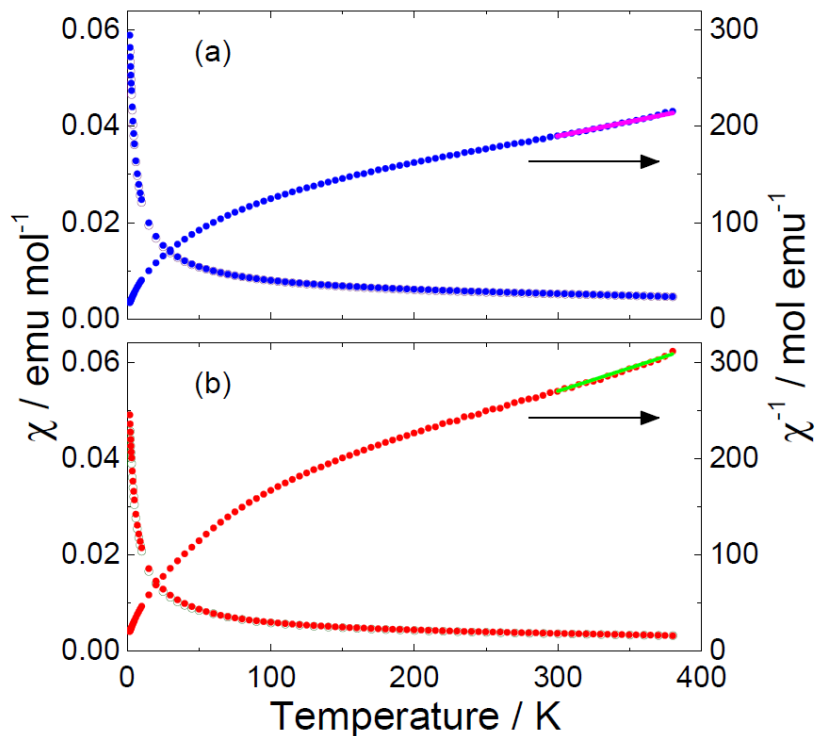


Figure 8 Molar magnetic susceptibility, χ and inverse magnetic susceptibility χ^{-1} as a function of temperature for (a) $\text{Ga}_{2.52}\text{V}_{2.48}\text{O}_{7.33}(\text{OH})_{0.67}$ and (b) $\text{Ga}_{2.52}\text{V}_{2.48}\text{O}_8$. The open symbols show the zero-field-cooled warming $\chi(T)$ data and the closed symbols show the field-cooled cooling data. The coloured lines are the Curie-Weiss fits referred to in the text.

$\chi(T)$ for both materials exhibit a paramagnetic behaviour over the temperature range studied (2 to 380 K). There is no hysteresis between the zero-field-cooled warming and field-cooled-cooling curves and no peaks or features in the data that would indicate the onset of magnetic order in either sample. Superficially, and especially at higher temperature, both materials appear to follow a Curie-Weiss behaviour, Equation (1),

$$\chi(T) = \left(\frac{C}{T - \theta_W} \right) + \chi_0 \quad \text{Equation 1,}$$

where C is the Curie constant and θ_w is the Weiss temperature. The $\chi^{-1}(T)$ curves (Figure 8), however, reveal the data are nonlinear, particularly below 200 K. This is expected for compounds containing V^{3+} ions in an octahedral crystal field [36, 37]. In this environment a d^2 metal ion with angular and spin quantum numbers $L = 3$ and $S = 1$, respectively, has a 3T_1 ground state and should have a temperature-dependent magnetic moment, according to Equation (2),

$$\bar{\mu}(T) = \left(\frac{3k_B}{N_A \mu_B} \right)^{\frac{1}{2}} (\chi T)^{\frac{1}{2}} \quad \text{Equation (2),}$$

where N_A is Avogadro's number, μ_B is the Bohr magneton, and k_B is Boltzmann's constant (see Figure 9). Using the van Vleck susceptibility and the appropriate results from perturbation theory in the weak crystal-field limit with a positive spin-orbit coupling parameter, λ_{SO} , it is anticipated that $\bar{\mu}$ will decrease from a value close to $\sim 2.7\mu_B$ per V^{3+} ion at room temperature to $0.62\mu_B$ per V^{3+} ion at $T = 0$ K according to Equation (3):

$$\bar{\mu}^2(T) = \frac{3 \left[0.625x + 6.8 + (0.125x + 4.09) \exp(-3x) - 10.89 \exp\left(-\frac{9x}{2}\right) \right]}{x \left[5 + 3 \exp(-3x) + \exp\left(-\frac{9x}{2}\right) \right]} \quad \text{Equation (3),}$$

where:

$$x = k_B T / |\lambda_{SO}| \quad \text{Equation (4).}$$

The observed temperature variation of $\bar{\mu}$ for both samples qualitatively follows this behaviour. The absolute values of $\bar{\mu}$ are lower than expected at higher temperature, perhaps indicating a spin-orbit coupling parameter that is significantly above the typical value of +150 K [37].

A magnetic susceptibility that gives rise to such a variation in $\bar{\mu}$ with temperature would appear to follow a Curie-Weiss law at higher temperature with a Weiss temperature of several hundred Kelvin [37], demonstrating that high values of θ_w do not necessarily have their origin in strong magnetic exchange. Since vanadium is distributed over sites also occupied by Ga any exchange between the V sites will be diluted by the diamagnetic Ga, so unless there is any local clustering of V no long-range correlations between V sites will be expected. Fitting the susceptibility data over a restricted temperature range between 300 and 380 K gives $C = (3.1 \pm 0.1) \text{ emu K Oe}^{-1} \text{ mol}^{-1}$ and $\theta_w = (-310 \pm 10) \text{ K}$ for the oxyhydroxide and $C = (2.2 \pm 0.05) \text{ emu K Oe}^{-1} \text{ mol}^{-1}$ and $\theta_w = (-270 \pm 15) \text{ K}$ for the oxide. This corresponds to an effective moment, p_{eff} , of $(3.16 \pm 0.05)\mu_B$ per V ion and $(2.66 \pm 0.05)\mu_B$ per V ion for $\text{Ga}_{2.52}\text{V}_{2.48}\text{O}_{7.33}(\text{OH})_{0.67}$ and the

$\text{Ga}_{2.52}\text{V}_{2.48}\text{O}_8$, respectively. These values are in reasonable agreement with the effective moment expected for a mixture of spin only V^{3+} ($2.83 \mu_{\text{B}}$) and V^{4+} ($1.73 \mu_{\text{B}}$) ions whose moments add in quadrature: for the oxyhydroxide, $p_{\text{eff}}^2 = [2.16(\mu_{\text{V}^{3+}})^2 + 0.32(\mu_{\text{V}^{4+}})^2]/2.48$ giving $p_{\text{eff}} = 2.71 \mu_{\text{B}}/\text{V}$ ion, while for the oxide $p_{\text{eff}}^2 = [1.48(\mu_{\text{V}^{3+}})^2 + 1.00(\mu_{\text{V}^{4+}})^2]/2.48$ giving $p_{\text{eff}} = 2.45 \mu_{\text{B}}/\text{V}$ ion. Magnetisation versus applied field, $M(H)$, curves at fixed temperature (5 and 300 K) shown in the inset of Figure 9 are consistent with $\chi(T)$ data. The samples appear paramagnetic at both temperatures. Although the magnetisation increases with decreasing temperature, the high-field magnetization at 5 K is far less than expected for a temperature independent moment. The $\chi(T)$ and $M(H)$ signals for the oxyhydroxide are higher than the equivalent data for the oxide, which is consistent with there being more V^{3+} in the $\text{Ga}_{2.52}\text{V}_{2.48}\text{O}_{7.33}(\text{OH})_{0.67}$ sample.

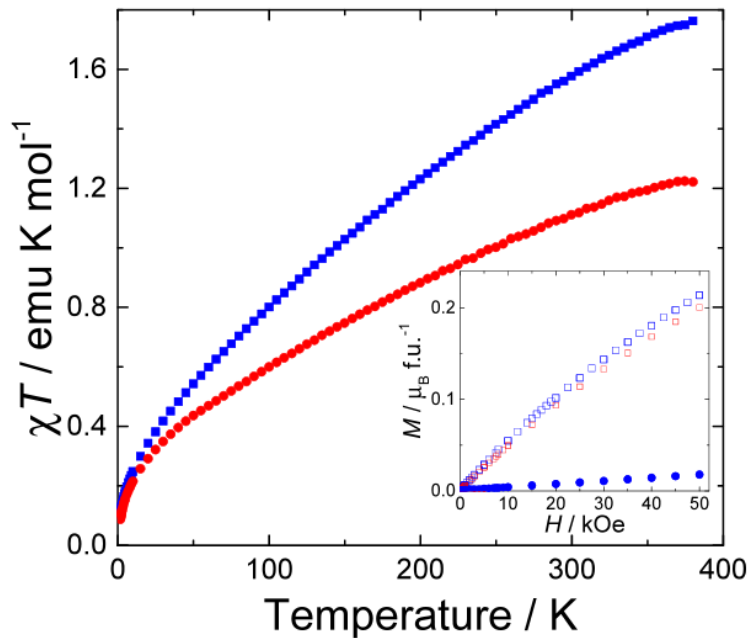


Figure 9: χT versus temperature for (squares) $\text{Ga}_{2.52}\text{V}_{2.48}\text{O}_{7.33}(\text{OH})_{0.67}$ and (circles) $\text{Ga}_{2.52}\text{V}_{2.48}\text{O}_8$. Both curves are field-cooled cooling data. The inset shows the magnetisation versus applied field. The open symbols show the data collected at 5 K and the closed symbols indicate the data collected at 300 K.

4. Conclusions

The solvothermal reaction between gallium metal (with a melting point of 29.5°C) and sodium orthovanadate in a mixed organic-aqueous solvent provides a convenient method to a new vanadium-gallium oxyhydroxide that can be thermally decomposed into a ternary oxide that contains mixed-valent vanadium. Despite using a V(V) -containing precursor, reduction takes

place to yield a V(III)-containing product under the synthesis conditions used. The structural investigation confirms the structural similarity of the oxyhydroxide to mineral phases, while XANES spectroscopy and magnetisation measurements are consistent with the assignment of vanadium oxidation state. The solvothermal synthesis method could be extended to other mixed oxides of gallium, or indeed to other low-melting point metals, to form precursors for the formation of new mixed-metal oxides that might otherwise be inaccessible.

Acknowledgements

DSC is grateful to Johnson Matthey plc for award of a studentship. We thank ISIS for provision of neutron diffraction beamtime (RB1610195) and Dr Helen Playford for assistance with measuring the data there, Diamond Light Source for award of XAFS beamtime (experiment SP13841), and Mr David Hammond for measuring thermogravimetric data. Some of the equipment used in this work was provided by the University of Warwick's Research Technology Platforms.

References

- [1] W.H. Barnes, M.M. Qurashi, Unit cell and space group data for certain vanadium minerals, *Am. Mineral.* 37 (1952) 407–422.
- [2] S.C. Robinson, H.T. Evans, W.T. Schaller, J.J. Fahey, Nolanite, a new iron-vanadium mineral from Beaverlodge, Saskatchewan, *Am. Mineral.*, 42 (1957) 619–628.
- [3] A. Hanson, The crystal structure of nolanite, *Acta Crystallogr.* 11 (1958) 703-709.
- [4] B.M. Gatehouse, I.E. Grey, E.H. Nickel, The crystal chemistry of nolanite, (V,Fe,Ti,Al)₁₀O₁₄(OH)₂, from Kalgoorlie, Western Australia, *Am. Mineral.*, 68 (1983) 833–839.
- [5] Z. Johan, P. Picot, Kamiokite, Fe₂Mo₃O₈, a tetravalent molybdenum oxide - new data and occurrences, *Tscher. Mineral. Petr. Mitt.* 35 (1986) 67-75.
- [6] C. Ma, J.R. Beckett, Majindeite, Mg₂Mo₃O₈, a new mineral from the Allende meteorite and a witness to post-crystallization oxidation of a Ca-Al-rich refractory inclusion, *Am. Mineral.* 101 (2016) 1161-1170.
- [7] X.D. Zhang, W.S. Yan, Y. Xie, Synthetic nolanite Fe_{2.5}V_{1.5}V_{5.6}O₁₆ nanocrystals: a new room-temperature magnetic semiconductor with semiconductor-insulator transition, *Chem. Commun.* 47 (2011) 11252-11254.
- [8] Y.P. Shpanov, G.A. Sidorenko, T.I. Stolyarova, Akdalaite, a new hydrated variety of alumina, *Int. Geol. Rev.* 13 (1971) 675-680.
- [9] G. Yamaguchi, H. Yanagida, S. Ono, The Crystal Structure of Tohdite, *Bull. Chem. Soc. Jpn.* 37 (1964) 1555-1557.
- [10] S.-L. Hwang, P. Shen, H.-T. Chu, T.-F. Yui, A New Occurrence and New Data on Akdalaite, a Retrograde Mineral from UHP Whiteschist, Kokchetav Massif, Northern Kazakhstan, *Int. Geol. Rev.* 48 (2006) 754-764.

- [11] G. Yamaguchi, M. Okumiya, S. Ono, Refinement of the structure of tohdite $5\text{Al}_2\text{O}_3 \cdot \text{H}_2\text{O}$, *Bull. Chem. Soc. Jpn.* 42 (1969) 2247-2249.
- [12] F.M. Michel, L. Ehm, S.M. Antao, P.L. Lee, P.J. Chupas, G. Liu, D.R. Strongin, M.A.A. Schoonen, B.L. Phillips, J.B. Parise, The structure of ferrihydrite, a nanocrystalline material, *Science* 316 (2007) 1726-1729.
- [13] J.B. Parise, B. Xia, J.W. Simonson, W.R. Woerner, A.M. Plonka, B.L. Phillips, L. Ehm, Structural Chemistry of Akdalaite, $\text{Al}_{10}\text{O}_{14}(\text{OH})_2$, the Isostructural Aluminum Analogue of Ferrihydrite, *Crystals* 9 (2019) 246.
- [14] H.Y. Playford, A.C. Hannon, E.R. Barney, R.I. Walton, Structures of Uncharacterised Polymorphs of Gallium Oxide from Total Neutron Diffraction, *Chem. Eur. J.* 19 (2013) 2803-2813.
- [15] H.Y. Playford, A.C. Hannon, M.G. Tucker, M.R. Lees, R.I. Walton, Total neutron scattering investigation of the structure of a cobalt gallium oxide spinel prepared by solvothermal oxidation of gallium metal, *J. Phys.: Condens. Matter* 25 (2013).
- [16] D.L. Burnett, M.H. Harunsani, R.J. Kashtiban, H.Y. Playford, J. Sloan, A.C. Hannon, R.I. Walton, Investigation of some new hydro(solvo)thermal synthesis routes to nanostructured mixed-metal oxides, *J. Solid State Chem.* 214 (2014) 30-37.
- [17] D.S. Cook, R.J. Kashtiban, K. Krambrock, G.M. de Lima, H.O. Stumpf, L.R.S. Lara, J.D. Ardisson, R.I. Walton, Nanocrystalline Transition-Metal Gallium Oxide Spinel from Acetylacetonate Precursors via Solvothermal Synthesis, *Materials* 12 (2019).
- [18] A.A. Coelho, TOPAS and TOPAS-Academic: an optimization program integrating computer algebra and crystallographic objects written in C plus, *J. Appl. Crystallogr.* 51 (2018) 210-218.
- [19] R.I. Smith, S. Hull, M.G. Tucker, H.Y. Playford, D.J. McPhail, S.P. Waller, S.T. Norberg, The upgraded Polaris powder diffractometer at the ISIS neutron source, *Rev. Sci. Instrum.* 90, (2019) 115101.
- [20] A.J. Dent, G. Cibir, S. Ramos, A.D. Smith, S.M. Scott, L. Varandas, M.R. Pearson, N.A. Krumpa, C.P. Jones, P.E. Robbins, B18: A core XAS spectroscopy beamline for Diamond, *J. Phys. Conf. Ser.*, 190, (2009) 12039.
- [21] B. Ravel, M. Newville, ATHENA, ARTEMIS, HEPHAESTUS: data analysis for X-ray absorption spectroscopy using IFEFFIT, *J. Synchrotron Rad.* 12 (2005) 537-541.
- [22] R. Demichelis, Y. Noel, C.M. Zicovich-Wilson, C. Roetti, L. Valenzano, R. Dovesi, Ab-initio quantum mechanical study of akdalaite ($5\text{Al}_2\text{O}_3 \cdot \text{H}_2\text{O}$): Structure and vibrational spectrum, *J. Phys.: Conf. Ser.* 117 (2008) 012013.
- [23] S. Geller, Crystal Structure of $\beta\text{-Ga}_2\text{O}_3$, *J. Chem. Phys.* 33 (1960) 676-684.
- [24] P.N. Anantharamaiah, P.A. Joy, Effect of size and site preference of trivalent non-magnetic metal ions (Al^{3+} , Ga^{3+} , In^{3+}) substituted for Fe^{3+} on the magnetostrictive properties of sintered CoFe_2O_4 , *J. Phys. D: Appl. Phys.* 50 (2017).
- [25] Y.O. Zagorodniy, V. Chlan, H. Stepankova, Y. Fomichov, J. Pejchal, V.V. Laguta, M. Nikl, Gallium preference for the occupation of tetrahedral sites in $\text{Lu}_3(\text{Al}_{5-x}\text{Ga}_x)\text{O}_{12}$ multicomponent garnet scintillators according to solid-state nuclear magnetic resonance and density functional theory calculations, *J. Phys. Chem. Solids* 126 (2019) 93-104.
- [26] Q.E. Stahl, G.J. Redhammer, G. Tippelt, A. Reyer, Structural and spectroscopic characterization of the brownmillerite-type $\text{Ca}_2\text{Fe}_{2-x}\text{Ga}_x\text{O}_5$ solid solution series, *Phys. Chem. Miner.* 46 (2019) 271-298.
- [27] B. Lavina, L.Z. Reznitskii, F. Bosi, Crystal chemistry of some Mg, Cr, V normal spinels from Sludyanka (Lake Baikal, Russia): the influence of V^{3+} on structural stability, *Phys. Chem. Miner.* 30 (2003) 599-605.
- [28] N.E. Brese, M. O'Keefe, Bond-Valence Parameters for Solids, *Acta Crystallogr. Sect B* 47 (1991) 192-197.

- [29] R.L. Richards, Vanadium: Inorganic & Coordination Chemistry in: R.A. Scott (Ed.), Encyclopedia of Inorganic Chemistry, John Wiley & Sons, Ltd Hoboken, New Jersey, United States, 2006, pp. 1-11.
- [30] A.C. Santulli, W.Q. Xu, J.B. Parise, L.S. Wu, M.C. Aronson, F. Zhang, C.Y. Nam, C.T. Black, A.L. Tiano, S.S. Wong, Synthesis and characterization of V₂O₃ nanorods, Physical Chemistry Chemical Physics 11 (2009) 3718-3726.
- [31] C.M. Zheng, X.M. Zhang, S. He, Q. Fu, D.M. Lei, Preparation and characterization of spherical V₂O₃ nanopowder, J. Solid State Chem. 170 (2003) 221-226.
- [32] F. Sediri, N. Gharbi, Hydrothermal synthesis and characterization of V₂O₃, Mater. Sci. Eng., B 123 (2005) 136-138.
- [33] I. Mjejri, A. Rougier, M. Gaudon, Low-Cost and Facile Synthesis of the Vanadium Oxides V₂O₃, VO₂, and V₂O₅ and Their Magnetic, Thermochromic and Electrochromic Properties, Inorg. Chem. 56 (2017) 1734-1741.
- [34] G.A. Bain, J.F. Berry, Diamagnetic Corrections and Pascal's Constants, J. Chem. Ed. 85 (2008) 532-536.
- [35] Quantum Design MPMS Application Notes 1014-201 and 1014-213, 2000.
- [36] B.N. Figgis, Magnetic Properties of Spin-Free Transition Series Complexes, Nature 182 (1958) 1568-1570.
- [37] F.E. Mabbs, D.J. Machin, Magnetism and Transition Metal Complexes, Chapman Hall, London, 1973.